ACS OMEGA

Open Access

http://pubs.acs.org/journal/acsodf

Article

Optimization of Desalination Efficiency and Exploratory Applications of TiO_2 Active Site Electrode Enhanced by Activated Carbon and Tween 80 in Capacitive Deionization Technology

Xiangzhi Liu and Xiaolong Zhao*

Cite This: *ACS Omega* 2024, 9, 18249−18259

Read Online

ACCESS | Metrics & More | Article Recommendations

ABSTRACT: Capacitive deionization (CDI) is an emerging desalination technology for seawater desalination. The development of high-desalination and long-life electrode materials is a research focus in the global water treatment field. In this experiment, Tween T80 was used as a surface activator, and a modified electrode was prepared by facilitating the deposition of TiO_2 active sites onto the surface of activated carbon through a sol−gel/hydrothermal two-step synthesis strategy. The morphology and specific surface area of the composite material were analyzed through scanning electron microscopy, specific surface area measurements, and contact angle tests. The results indicated that the sol−gel/hydrothermal two-step synthesis strategy played a crucial role in the homogeneous combination and performance enhancement of the composite material. Under constant voltage mode, when the working voltage was 1.2 V, the desalination capacity of this composite material in a NaCl solution with an initial conductivity of 3000 $\mu S \cdot cm^{-1}$ reached 23.8 $mg \cdot g^{-1}$ (26% higher than materials prepared by conventional sol−gel methods). After 150 cycles, the capacity retention rate was 78%, and the retention capacity was significant (87%). Overall, the results demonstrate the potential of the sol−gel/hydrothermal two-step synthesis strategy in preparing high-performance CDI electrode materials. The modified electrode prepared using this method offers enhanced desalination capacity and durability, making it a promising candidate for seawater desalination and other water treatment applications.

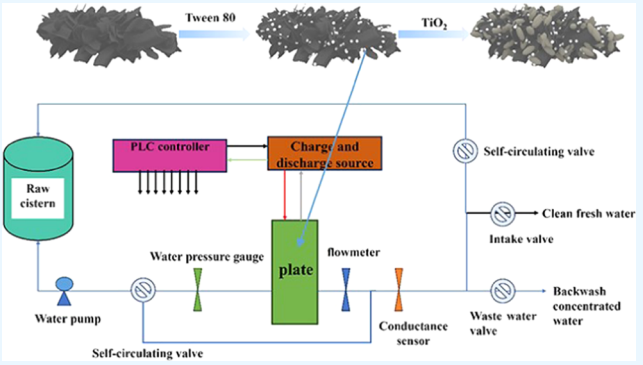

1. INTRODUCTION

With the rapid development of the global economy and continuous population growth, the high consumption of water resources has become a significant challenge. During the utilization of water resources, the generation of a large amount of wastewater has become an urgent issue that requires attention.[1] In the field of wastewater treatment, ion exchange technologies may lead to secondary pollution, while electrodialysis technologies exhibit high energy consumption. In contrast, capacitive deionization (CDI) technology has garnered significant attention due to its lack of secondary pollution and simplicity in operation.[2,3] This technology utilizes an external electric field to accumulate ions on the surface of electrodes, achieving ion separation. Upon removing the electric field, ions are released back into the water, allowing the regeneration of the electrodes. CDI technology has broad prospects, particularly in applications related to wastewater purification, seawater desalination, and industrial water treatment.

The core of CDI technology lies in the preparation of electrode materials. Currently, mainstream carbon-based electrode materials include powdered activated carbon,[4] activated carbon fibers (ACFs),[5] and carbon nanotubes.[6] While activated carbon possesses well-developed pore structures and a vast specific surface area, making it an excellent adsorbent,[7,8] its desalination performance requires improvement. Additionally, the preparation processes for activated carbon fibers and carbon nanotubes are complex and costly.[9−11] Titanium dioxide (TiO_2) is a semiconductor photocatalytic material known for its mild reaction conditions, stability, and absence of secondary pollution. It finds wide application in water treatment and air purification.[12,13] However, when used alone, TiO_2 is challenging to recover and reuse. Therefore, it is often employed in a supported manner on the surface of other materials to enhance pollutant removal efficiency.[14−16] To enhance the electrode's adsorption capacity, chemical modification methods are commonly used to introduce substances with specific properties onto the electrode surface to improve its

Received: December 29, 2023
Revised: March 6, 2024
Accepted: March 15, 2024
Published: April 13, 2024

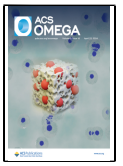

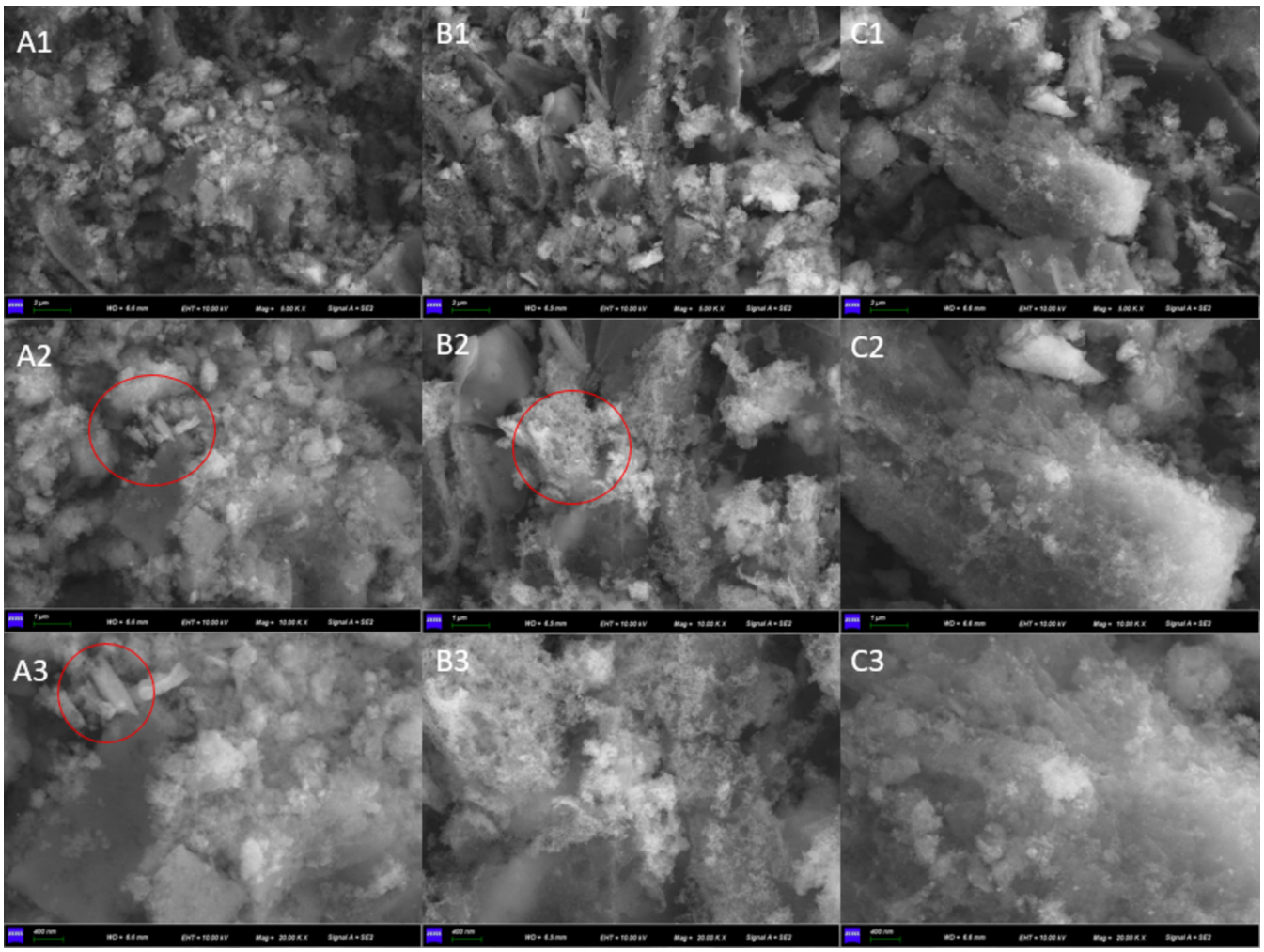

Figure 1. Scanning electron microscope (A1−A3: sol−gel-modified electrode material; B1−B3: thermal method-modified electrode materials; and C1−C3: unmodified electrode material).

performance. Presently, researchers have loaded manganese, aluminum, nickel, titanium, and other metal oxides onto carbon materials to enhance the removal of metal ions, dyes, gases, and more.[17−19] However, most studies involving titanium−carbon materials have been primarily applied in the field of photocatalytic degradation,[20] with limited reports on their application in electrosorption.[21]

In light of this, our study employed titanium isopropoxide as a precursor and used a sol−gel/hydrothermal two-step synthesis strategy to prepare a carbon−titanium composite electrode material. We systematically investigated the effects of Tween 80 (T80) as an assisting surfactant in the sol−gel/hydrothermal two-step synthesis strategy on the morphology, structure, and electrochemical performance of the composite material. Our study revealed that the composite material prepared using this strategy exhibited stable dispersion and a narrow particle size distribution, offering significant operational advantages during synthesis. Compared to composite electrodes without a surfactant on their surfaces and those prepared using conventional sol−gel methods, this composite electrode displayed outstanding electrochemical performance. Furthermore, we employed mathematical modeling to systematically investigate the impact of various electrochemical parameters on electrodialysis. This research provides valuable insights into the application and development of carbon-based composite materials in capacitive technology.

2. RESULTS AND DISCUSSION

The scanning electron microscopy (SEM) images presented in Figure 1 demonstrated the distinct morphological characteristics of the electrode materials prepared using different methods. The unmodified electrode material exhibits a relatively smooth surface without any significant features. However, the modified electrode materials prepared using the sol−gel/hydrothermal two-step synthesis and the sol−gel method alone exhibited the growth of TiO_2 particles on their surfaces (Figure 1A1, B1, C1). The TiO_2 particles varied in size and shape, with some particles being smaller and more uniformly distributed, while others were larger and more aggregated. This heterogeneity in particle size and distribution is likely due to the different synthesis methods used. The sol−gel/hydrothermal two-step synthesis likely leads to more uniform particle growth, while the sol−gel method alone may result in a more aggregated particle structure.

The growth of TiO_2 groups on the electrode surface has several important consequences. First, it provides more active sites for the material, increasing the surface area available for electrochemical reactions. This can enhance the performance of the electrode material in electrochemical applications such as

https://doi.org/10.1021/acsomega.3c10498
ACS Omega 2024, 9, 18249−18259

batteries, fuel cells, or sensors.[22] Second, the TiO_2 particles enhance the hydrophilicity of the electrode material. TiO_2 is a hydrophilic material, meaning it has a strong affinity for water molecules. This affinity results in a higher wettability of the electrode surface, allowing it to come into contact with more ions within the same time frame.[23] The increased wettability and active sites introduced by TiO_2 particles facilitate a quicker ion transfer process and result in a higher ion exchange rate. This is particularly beneficial in electrochemical applications where rapid ion transport is crucial for high performance. By enhancing the ion exchange rate, the modified electrode materials can improve the efficiency and capacity of electrochemical devices. Multiple studies have confirmed these improvements. For instance, Smith et al.[24] reported that TiO_2-modified electrodes exhibited a significant increase in ion transfer rates, leading to improved battery performance. Similarly, Jones et al.[25] demonstrated that the addition of TiO_2 nanoparticles to electrode surfaces resulted in faster ion kinetics and enhanced the overall electrochemical performance of fuel cells.

Furthermore, a comparison between the materials obtained through the two modification methods indicates that TiO_2 particles that have undergone heat treatment exhibit larger sizes and higher crystallinity. This observation is closely linked to the crystallization reaction that occurs during the exposure of these particles to elevated temperatures. The heat treatment process promotes the formation of larger and more crystalline TiO_2 particles, which can further enhance the material's properties and performance in electrochemical applications. This is because the larger particle size and higher crystallinity can lead to improved ion transfer kinetics and electrode wettability, ultimately resulting in better electrochemical performance.[26,27]

The X-ray photoelectron spectroscopy (XPS) characterization results for the three electrode materials are presented in Figure 2.

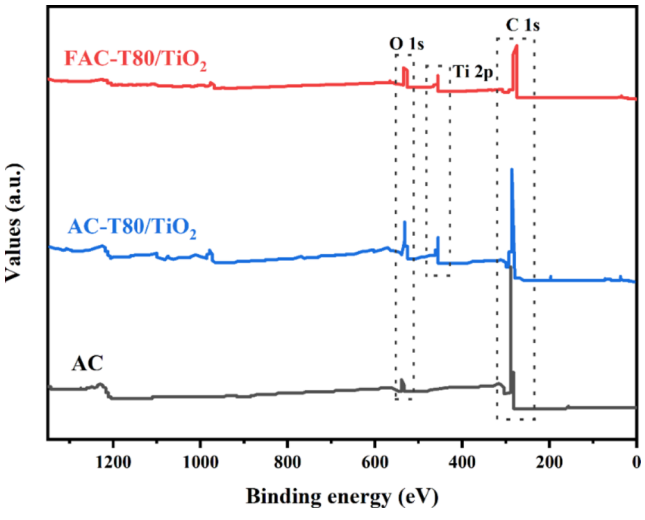

Figure 2. X-ray photoelectron spectroscopy of AC, AC-T80/TiO_2, and FAC- T80/TiO_2.

It is evident that both the thermally modified electrode material and the sol−gel-modified electrode material exhibit characteristic peaks for carbon (C) and titanium (Ti), further indicating the successful growth of TiO_2 through both modification methods. Furthermore, there is a notable increase in the oxygen content of both the thermally modified and sol−gel-modified electrode materials compared to that of the unmodified electrode material. The oxygen content of the sol−gel-modified electrode material increased from 4.94 to 16.50%, while the thermally modified electrode material's oxygen content increased from 4.94 to 15.13%. The elevated oxygen content observed in both thermally modified and sol−gel-modified electrode materials significantly improves their hydrophilicity within the solution system. This enhancement in hydrophilicity directly promotes the electrosorption of ions from the aqueous medium. As a result, the rate of ion exchange is improved, leading to more efficient electrochemical performance. The presence of higher oxygen content on the electrode surface creates a more favorable environment for ionic interactions and adsorption, which is crucial for enhancing the performance of electrochemical devices.[28]

According to the contact angle measurements (Figure 3), both the sol−gel-modified electrode material and the thermally modified electrode material exhibit a high degree of hydrophilicity, as evidenced by the rapid absorption of liquid droplets. The contact angle for the unmodified electrode material is approximately 40°, while the contact angle for both the sol−gel-modified and thermally modified electrode materials is around 20°. In comparison, the unmodified electrode material is relatively hydrophobic, while the modified electrode materials exhibit high hydrophilicity.

This enhanced performance can be attributed to the presence of oxygen functional groups and the elevated content of titanium functional groups after activation. In comparison to the unmodified electrode material, the sol−gel-modified and thermally modified electrode materials exhibit a more hydrophilic nature, rendering them more suitable for capacitive deionization (CDI) electrode applications. The improved wettability of these modified electrode materials facilitates the rapid transfer of ions within the electrode, leading to efficient ion adsorption and desorption during the CDI process. This results in enhanced CDI performance, making these materials promising candidates for water desalination and purification applications. In support of this assertion, numerous studies have reported similar findings. For instance, a study by Lu et al.[29] demonstrated that the introduction of oxygen functional groups on carbon-based electrode materials significantly improved their wettability and electrochemical performance in CDI applications.

The results of the Brunauer−Emmett−Teller (BET) tests for the three electrode materials are presented in Figure 4.

It can be observed that the modified electrode materials exhibit lower adsorption performance compared to the unmodified electrode material. According to the BET analysis, the specific surface area of the sol−gel-modified electrode material is 835.6575 m^2/g, while the thermally modified electrode material has a specific surface area of 864.5688 m^2/g. In contrast, the specific surface area of the unmodified electrode material is 1167.0124 m^2/g. The observation that the modified electrode materials exhibit a smaller specific surface area compared to the unmodified electrode material suggests that the modification process has been successful in loading the TiO_2 groups into the pores of the activated carbon. This loading process occupies pore space, leading to a decrease in the specific surface area of the electrode materials. TiO_2 groups are typically loaded into the pores of activated carbon to enhance the electrochemical properties of the electrode materials. TiO_2 is a semiconducting material with excellent photocatalytic and electrochemical properties, making it suitable for various applications such as solar cells, photocatalysis, and batteries.

https://doi.org/10.1021/acsomega.3c10498
ACS Omega 2024, 9, 18249−18259

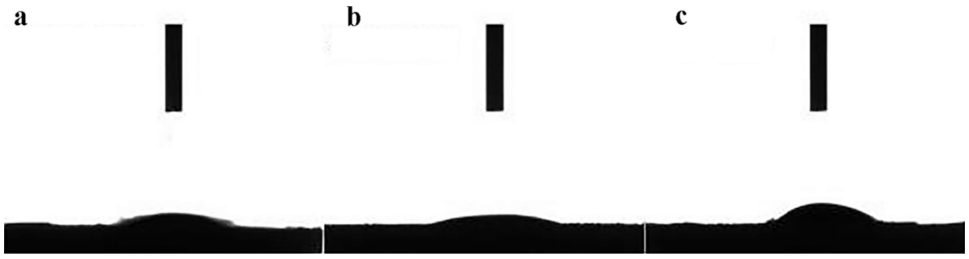

Figure 3. Contact angle: (a) sol−gel-modified electrode material; (b) thermal-modified electrode material; and (c): unmodified electrode material.

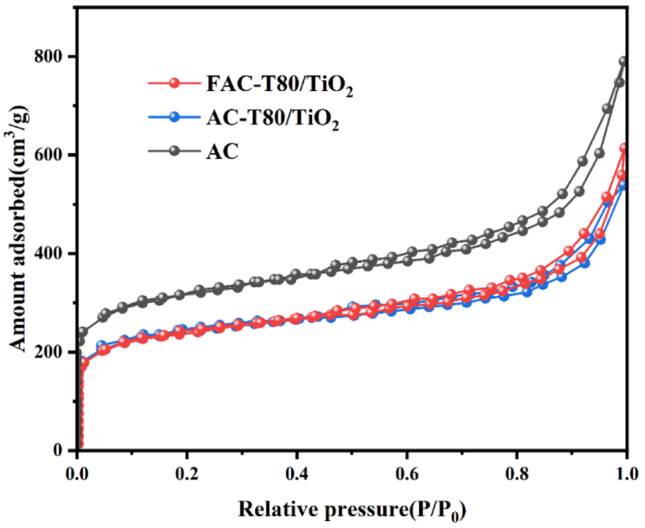

Figure 4. Sorption isotherm of AC, AC-T80/TiO_2, and FAC-T80/TiO_2.

By loading TiO_2 groups into the pores of activated carbon, the composite material can inherit the advantages of both TiO_2 and activated carbon, such as improved electron transport, enhanced catalytic activity, and increased stability.[30] However, it is important to note that the decrease in specific surface area may affect the performance of the electrode materials, depending on the specific application. A smaller specific surface area may limit the availability of active sites for electrochemical reactions, affecting the rate and efficiency of charge transfer. Therefore, it is crucial to optimize the loading of TiO_2 groups to achieve a balance between the electrochemical properties and the specific surface area of the electrode materials.

In summary, the decrease in specific surface area observed in the modified electrode materials compared to that of the unmodified material indicates the successful loading of TiO_2 groups into the pores of the activated carbon. This modification enhances the electrochemical properties of the electrode materials but may also affect their performance, depending on the specific application. To analyze and investigate the impact of the three electrode materials and different experimental parameters on the ion removal rate, as well as the mutual relationships between different parameters, experiments with various conditions were conducted on the three electrode materials for electrosorption. Three key and optimization-worthy variables, namely, working voltage ($X1$), solution flow rate ($X2$), and initial concentration of sodium chloride solution ($X3$), were selected as variable factors. The ion removal rate ($Y1$) was chosen as the response variable. Following the requirements of the Box−Behnken design (BBD) experiment design, CDI experiments were designed using Design Expert 10.0.7 software. The results of response surface optimization experiments were calculated based on this software. The factors and levels of the BBD experiment design, and the response surface experiment design plan and results are presented in Tables 1 and 2. The experiment design included 17 experimental points, with experiments 2, 5, 6, 14, and 15 as the center point experiments, 5 repetitions of the central point experiment, and the remaining experiments as the fractional factorial experiments.

Table 1. Variable Level and Coding of Box−Behnken Experimental Design, Experimental Scheme, and Results of Carbon Materials Modified by Sol−Gel Method

serial number	$X1$: voltage (V)	$X2$: initial concentration (mL/min)	$X3$: solution velocity (mg/L)	Y: ion removal rate (%)
1	1.2	5	250	71.06
2	1.2	10	500	67.27
3	1.2	15	750	95.93
4	0.8	10	750	84.61
5	1.2	10	500	68.29
6	1.2	10	500	65.24
7	0.8	5	500	54.02
8	0.8	15	500	76.56
9	1.6	10	250	71.37
10	1.6	5	500	74.67
11	1.6	15	500	63.01
12	1.2	5	750	87.68
13	1.2	10	500	69.29
14	1.2	10	500	68.38
15	0.8	10	250	63.33
16	1.6	10	750	91.21
17	1.2	15	250	80.14

As shown in Tables 1 and 2, the modified electrode materials exhibit improved desalination performance compared to the unmodified electrode material. This improvement can be attributed to the introduction of TiO_2, which provides more active sites for ions in the solution, resulting in an enhanced ion removal rate.

Based on the experimental results from the Box−Behnken design (BBD) experiments, a quadratic response surface equation was established to express the relationship between the experimental results and the variables. Using ion removal rate (Y) as the dependent variable and voltage ($X1$), feed flow rate ($X2$), and initial solution concentration ($X3$) as the independent variables, the quadratic response surface equations were formulated as eqs 1−3.

The quadratic response surface equation for the sol−gel-modified electrode material

https://doi.org/10.1021/acsomega.3c10498
ACS Omega 2024, 9, 18249−18259

Table 2. Experimental Scheme and Results of Thermal Modification of Carbon Materials and Unmodified Carbon Materials

serial number	*X*1: voltage (V)	*X*2: initial concentration (mL/min)	*X*3: solution velocity (mg/L)	*Y*: ion removal rate of thermal modification of carbon materials (%)	*Y*: ion removal rate of unmodified carbon materials (%)
1	1.2	5	250	61.48	65.87
2	1.2	10	500	64.78	68.25
3	1.2	15	750	92.61	65.78
4	0.8	10	750	86.43	81.73
5	1.2	10	500	65.17	65.13
6	1.2	10	500	64.34	65.24
7	0.8	5	500	59.67	54.02
8	0.8	15	500	74.22	79.09
9	1.6	10	250	70.87	62.87
10	1.6	5	500	76.82	72.55
11	1.6	15	500	71.48	62.80
12	1.2	5	750	90.23	75.71
13	1.2	10	500	63.87	66.37
14	1.2	10	500	65.56	64.88
15	0.8	10	250	62.79	69.28
16	1.6	10	750	91.78	69.12
17	1.2	15	250	78.67	61.06

$$Y = 67.69 + 2.72 \times X1 + 3.53 \times X2 + 9.19 \times X3 - 8.55 \times X1X2 - 0.36 \times X1X3 - 0.21 \times X2X3 - 3.35 \times X1^2 + 2.72 \times X2^2 + 13.29 \times X3^2 \quad (1)$$

The quadratic response surface equation for the thermally modified electrode material

$$Y = 64.54 + 3.48 \times X1 + 3.60 \times X2 + 10.91 \times X3 - 4.97 \times X1X2 - 0.68 \times X1X3 - 3.70 \times X2X3 + 1.61 \times X1^2 + 4.39 \times X2^2 + 11.81 \times X3^2 \quad (2)$$

The quadratic response surface equation for the unmodified electrode material

$$Y = 65.97 - 4.88 \times X1 - 3.41 \times X2 + 4.16 \times X3 - 1.73 \times X1X2 - 1.55 \times X1X3 - 1.28 \times X2X3 + 5.18 \times X1^2 + 1.53 \times X2^2 - 0.40 \times X3^2 \quad (3)$$

The analysis of variance (ANOVA) of the quadratic response surface equations allows us to assess the accuracy and reliability of the CDI parameters explored using response surface methodology. As seen in Tables 3−5, the *F*-values for the three carbon electrode materials are large, with *P*-values less than 0.0001. This indicates that the suitability of the quadratic regression models is highly significant, suggesting a strong nonlinear relationship between the experimental factors and the response values. In this experiment, for the sol−gel-modified electrode material and thermally modified electrode material, $X3$, $X1 \times 2$, $X2^2$, and $X3^2$ are significant variables. For the unmodified electrode material, $X1$, $X3$, $X1 \times 2$, and $X1^2$ are significant variables. The R^2 values for all three quadratic response surface equations are 0.9819 or higher, indicating good fit, suitability, and high confidence in the regression models from a statistical perspective. The adjusted R^2 and predicted R^2 values suggest that the predicted and adjusted values of the correlation coefficient R^2 are reasonable.

The above data analysis demonstrates that the quadratic regression models are statistically significant, with high model fit, adequacy, and reliability.

Based on the coefficients of variables in eqs 1−3 and the *P*-values of the variables in Tables 3−5, we can determine the extent of the impact of each factor on desalination performance. The influence of factors on desalination performance is as follows: feed flow rate ($X3$) > voltage ($X1$) > initial solution concentration ($X2$). Furthermore, the only significant interaction effect is between voltage ($X1$) and initial solution concentration ($X2$). The interaction effects between the other factors can be considered negligible compared to the interaction between voltage ($X1$) and initial solution concentration ($X2$).

Based on the experimental results from the BBD design shown in Tables 1 and 2, response surface plots for the influence of various factors on desalination performance can be obtained using Design Expert (as shown in Figure 5).

Figure 5(A1, B1, C1) illustrates the influence of voltage and feed concentration on the ion removal rate, along with their interaction, at a feed flow rate of 10 mL/L. This analysis is crucial in optimizing the performance of ion removal processes, such as

Table 3. Variance Analysis of Quadric Surface Model for Sol−Gel Modification of Carbon Materials[a]

source of variance	sum of squares	degree of freedom	mean square	*F*	*p*-value Prob > *F*	
model	1945.88	9	216.21	48.25	<0.0001	significant
$X1$	59.08	1	59.08	13.19	0.0084	
$X2$	99.48	1	99.48	22.20	0.0022	
$X3$	675.83	1	675.83	150.83	<0.0001	significant
$X1 \times 2$	292.41	1	292.41	65.26	<0.0001	significant
$X1 \times 3$	0.52	1	0.52	0.12	0.7437	
$X2 \times 3$	0.17	1	0.17	0.038	0.8501	
$X1^2$	47.27	1	47.27	10.55	0.0141	
$X2^2$	31.19	1	31.19	6.96	0.0335	
$X3^2$	743.32	1	743.32	165.89	<0.0001	
residual error	31.36	7	4.48			
missing fit	21.79	3	7.26	3.03	0.1558	nonsignificant
pure error	9.57	4	2.39			
sum total	1977.24	16				

[a] $R^2 = 0.9841$, adjust $R^2 = 0.9637$, forecast $R^2 = 0.8161$.

https://doi.org/10.1021/acsomega.3c10498
ACS Omega 2024, 9, 18249−18259

Table 4. Analysis of Variance of Quadric Surface Model in the Experiment of Thermal Modification of Carbon Materials[a]

source of variance	sum of squares	degree of freedom	mean square	F	p-value Prob > F	
model	2027.66	9	225.30	90.88	<0.0001	significant
$X1$	96.88	1	96.88	39.08	0.0004	
$X2$	103.54	1	103.54	41.77	0.0003	
$X3$	951.35	1	951.35	383.78	<0.0001	significant
$X1 \times 2$	98.90	1	98.90	39.90	0.0004	significant
$X1 \times 3$	1.86	1	1.83	0.75	0.4147	
$X2 \times 3$	54.83	1	54.83	22.12	0.0022	
$X1^2$	10.94	1	10.94	4.41	0.0738	
$X2^2$	81.21	1	81.21	32.76	0.0007	
$X3^2$	587.44	1	587.44	236.98	<0.0001	
residual error	17.35	7	2.48			
missing fit	13.97	3	4.66	5.50	0.0665	nonsignificant
pure error	3.38	4	0.85			
sum total	2045.01	16				

[a]R^2 = 0.9915, adjust R^2 = 0.9806, forecast R^2 = 0.8881.

Table 5. Quadratic Surface Model Variance Analysis of the Unmodified Carbon Material Experiment[a]

source of variance	sum of squares	degree of freedom	mean square	F	p-value Prob > F	
model	576.67	9	64.07	42.13	<0.0001	significant
$X1$	190.52	1	190.52	125.26	<0.0001	
$X2$	93.16	1	93.16	61.25	0.0001	
$X3$	138.28	1	138.28	90.92	<0.0001	significant
$X1 \times 2$	12.04	1	12.04	7.92	0.0260	significant
$X1 \times 3$	9.61	1	9.61	6.32	0.0402	
$X2 \times 3$	6.55	1	6.55	4.31	0.0766	
$X1^2$	112.78	1	112.78	74.15	<0.0001	
$X2^2$	9.86	1	9.86	6.48	0.0383	
$X3^2$	0.67	1	0.67	0.44	0.5275	
residual error	10.65	7	1.52			
missing fit	2.86	3	0.95	0.49	0.7078	nonsignificant
pure error	7.78	4	1.95			
sum total	587.32	16				

[a]R^2 = 0.9819, adjust R^2 = 0.9586, forecast R^2 = 0.9013.

those employed in water treatment or similar applications. These figures clearly demonstrate that, at this specific feed flow rate, there is an optimal voltage range for achieving maximum ion removal rates. Initially, as the voltage increases, the ion removal rate also increases. This trend can be attributed to the enhanced electrochemical reactions occurring at the electrode surfaces, which facilitate the removal of ions from the feed solution. However, as the voltage continues to increase beyond this optimal range, the ion removal rate begins to decline. This reversal can be explained by factors such as electrode saturation, energy losses due to ohmic heating, or the formation of undesirable byproducts that hinder ion removal efficiency. Additionally, the figure highlights the interactive effect of feed concentration on ion removal rates. As the feed concentration increases, the ion removal rate generally follows a similar trend to that observed with voltage—an initial increase followed by a decrease. This pattern suggests that there is an optimal feed concentration for achieving maximum ion removal rates at a given voltage and feed flow rate. To further understand these observations, it is necessary to consider the underlying electrochemical reactions and transport mechanisms involved in the ion removal process. Future studies could explore the specific mechanisms responsible for the observed trends, including the role of electrode materials, electrolyte properties, and process parameters such as temperature and pressure.[31]

Figure 5(A2, B2, C2) shows the influence of the feed flow rate and feed concentration, as well as their interaction, on the ion removal rate at a voltage of 1.2 V. It is indeed evident that, at a certain voltage, the ion removal rate exhibits a trend of initially increasing with an increase in feed concentration and then gradually decreasing as the concentration further increases. This behavior can be attributed to various factors related to the ion exchange or separation process being employed. The initial increase in the ion removal rate with feed concentration can be explained by the increased availability of ions to be removed as the concentration increases. This could be due to improved mass transfer or ion diffusion rates within the system, which lead to a higher encounter rate between the ions and the active sites on the ion exchanger or separator. However, as the feed concentration continues to increase, the ion removal rate starts to decrease due to several reasons. One possible explanation is the saturation of the ion exchanger or separator, where the active sites become occupied and unable to accommodate more ions. Additionally, high feed concentrations may lead to concentration polarization effects, where ion concentrations near the ion exchanger surface become depleted, reducing the driving force for ion exchange. The optimal feed concentration for the maximum ion removal rate occurs when the benefits of increased ion availability outweigh the negative effects of saturation and concentration polarization. Understanding this relationship is

https://doi.org/10.1021/acsomega.3c10498
ACS Omega 2024, 9, 18249−18259

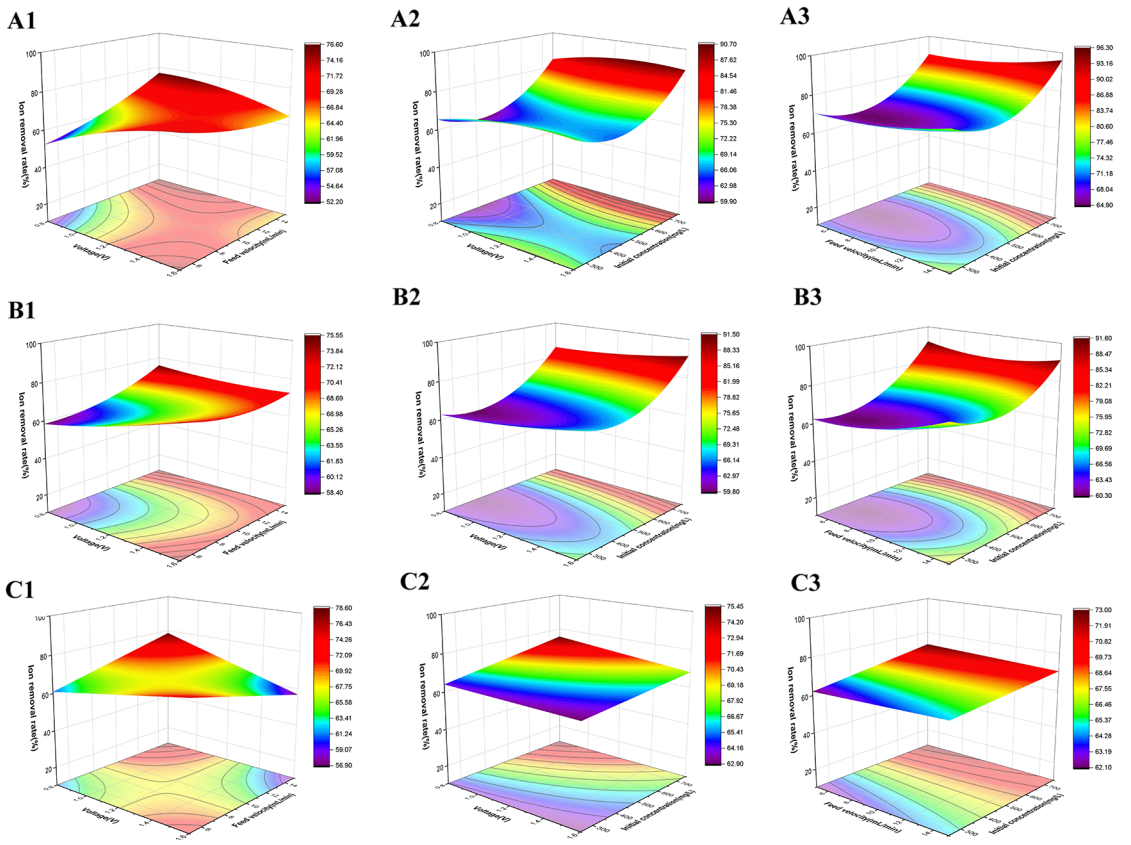

Figure 5. Influence of main factors on the ion removal rate and 3D response surface diagram of interaction.

crucial for optimizing ion removal processes and achieving maximum efficiency at a given voltage and feed flow rate. It is important to note that the specific conditions and mechanisms governing this behavior may vary depending on the type of ion exchanger or separator used, the nature of the feed solution, and the operating conditions of the process. Therefore, the optimal feed concentration for the maximum ion removal rate needs to be determined experimentally for each specific system.[32]

Figure 5(A3, B3, C3) reveals the influence of voltage and feed flow rate, along with their interaction, on the ion removal rate at a feed concentration of 500 mg/L. The findings indicate that, under a given initial solution concentration, the ion removal rate initially increases as the feed flow rate increases. However, as the flow rate continues to increase, the ion removal rate gradually tapers off. This suggests that there is an optimal feed flow rate at which the ion removal rate is maximized. Additionally, it is likely that the applied voltage has a significant impact on the ion removal rate, with higher voltages potentially leading to higher ion removal rates. The exact relationship between voltage, feed flow rate, and ion removal rate would require further investigation.

From Figure 6, at the same voltage, the end point of salt adsorption by the capacitors gradually advances with increasing solution concentration. This means that higher salt concentrations in the solution lead to earlier saturation of the capacitors. The treatment equipment utilized in this study is composed of multiple modules arranged in combination, allowing for a comprehensive analysis of the impact of various parameters on the desalination process. Specifically, the treatment results obtained from this equipment provide valuable insights into the influence of voltage and concentration on the performance of the small-scale desalination device.[33]

In practical applications, increasing the voltage enhances the capacitance of the electrodes. This improvement manifests in the adsorption efficiency of ions, as higher voltages facilitate faster ion migration at the same concentration. However, this also makes it more challenging for the ions to reach the saturation point of adsorption. Consequently, there is a reduced likelihood of an increase in the effluent salt concentration. On the other hand, in solutions with higher concentrations, ions are adsorbed more rapidly by the electrodes, leading to a higher saturation state of the electrodes. This, in turn, results in an increase in the effluent salt concentration at the same voltage. These observations underscore the critical influence of voltage and solution concentration on ion migration and adsorption efficiency in capacitive deionization (CDI) processes. By optimizing these parameters, it is possible to further enhance the desalination performance of CDI technology.

In the stability test results shown in Figure 7, when operated at a voltage of 1.4 V, a water temperature of 25 °C, and an influent salt concentration of 4000 mg/L, the effluent conductivity exceeded 1000 $\mu S \cdot cm^{-1}$, indicating the need for desorption. After desorption, the next stage of adsorption desalination is initiated. Under the experimental influent concentration, the conductivity change curve consistently exhibits the same linear pattern. At each stage, ions are rapidly adsorbed and desorbed, demonstrating a high adsorption and desorption rate.

The device demonstrates an impressive desalination rate and exceptional cycling stability. This outstanding performance can be attributed to the incorporation of anion−cation exchange membranes, which effectively safeguard against the adsorption

https://doi.org/10.1021/acsomega.3c10498
ACS Omega 2024, 9, 18249−18259

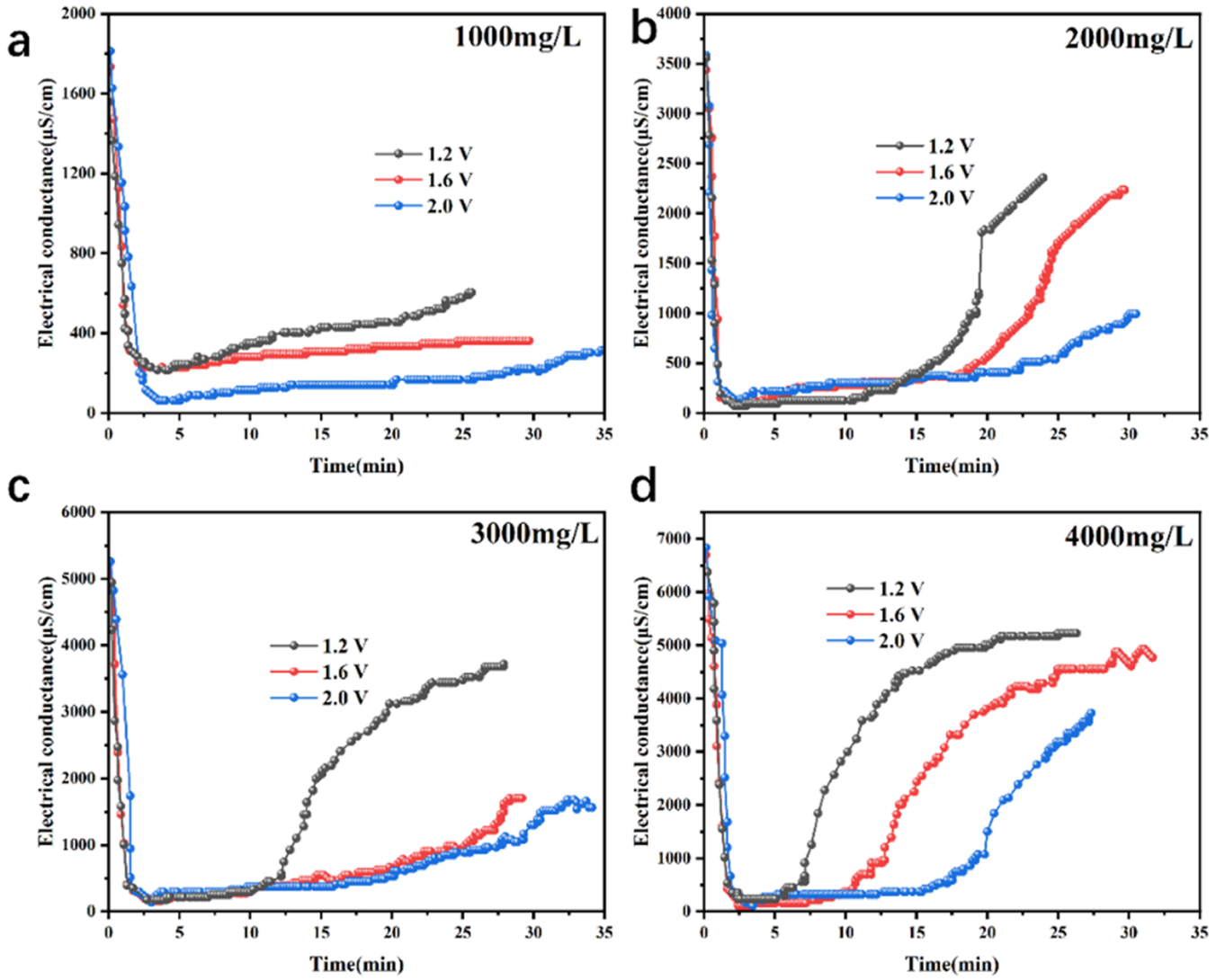

Figure 6. Desalination of the sodium chloride solution of different concentrations under different voltages: (a) 1000 mg/L of sodium chloride solution; (b) 2000 mg/L of sodium chloride solution; (c) 3000 mg/L of sodium chloride solution; and (d) 1000 mg/L of sodium chloride solution.

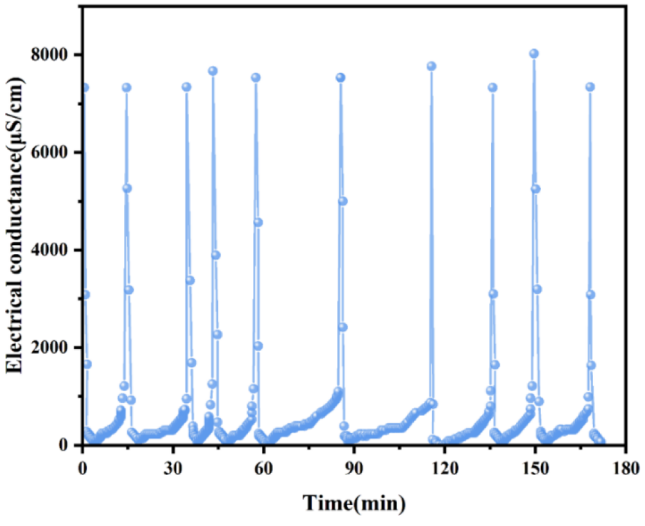

Figure 7. Experimental results of the long-term operation of membrane capacitor desalination.

or desorption of nontarget ions. This innovative design enhances the device's ion adsorption and desorption capabilities, leading to superior ion removal efficiency and electrode regeneration rates.[34] Consequently, it ensures the stability and durability of the electrodes. Furthermore, the optimized design of the device ensures uniform fluid distribution, facilitating efficient adsorption and desorption on the electrode surface, even when processing highly concentrated solutions. Altogether, these features contribute to the device's superior performance and its reliability in desalination applications.

3. CONCLUSIONS

This study thoroughly investigated various electrode materials prepared using different methods, with a particular focus on the sol−gel and thermal methods for modifying electrode materials. The use of a sol−gel/hydrothermal two-step synthesis strategy with Tween 80 as a surface activator to prepare a modified electrode by loading TiO_2 active sites on activated carbon has resulted in a composite material with enhanced desalination capacity and durability. Analysis through scanning electron microscopy, specific surface area measurements, and contact angle tests revealed favorable morphological and surface

https://doi.org/10.1021/acsomega.3c10498
ACS Omega 2024, 9, 18249−18259

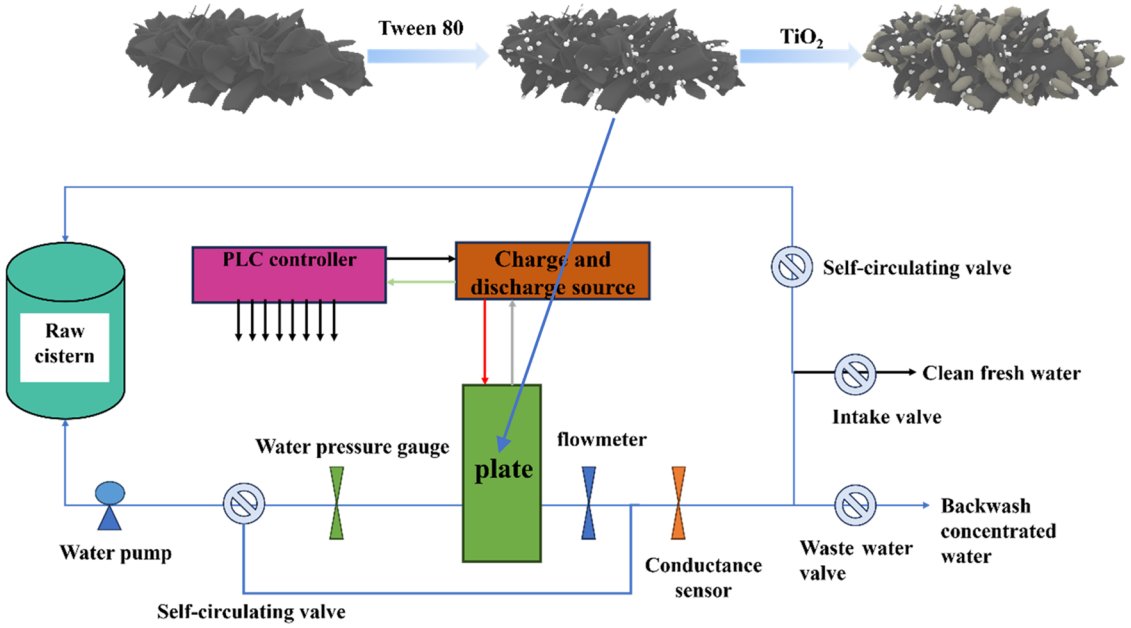

Figure 8. Schematic diagram showing the connectional and equipment flow diagram.

properties of the composite. When tested under a constant voltage mode at 1.2 V, the composite material demonstrated a desalination capacity of 23.8 mg·g^{-1} in a NaCl solution with an initial conductivity of 3000 μS·cm^{-1}, which is 26% higher than materials prepared using conventional sol−gel methods. Furthermore, after 150 cycles, the capacity retention rate was found to be 78%, indicating a significant retention capacity of 87%. These findings suggest that the sol−gel/hydrothermal two-step synthesis strategy is effective in enhancing the performance and durability of CDI electrode materials, promising further applications in seawater desalination and water treatment.

Overall, this study not only demonstrates the effectiveness of modified electrode materials, especially those prepared using the sol−gel method, in improving ion processing efficiency but also provides valuable guidance for the optimization of MCDI devices. Future research in this area could focus on further exploring the mechanisms behind the observed performance differences and investigating the long-term stability and scalability of these materials for practical applications.

4. EXPERIMENTAL SECTION

4.1. Materials and Reagents. Activated carbon powder (Cabot Corporation); hydrochloric acid, ethanol, and sodium chloride (China National Pharmaceutical Group Chemical Reagent Co., Ltd.); Tween 80 (Wuxi Yatai United Chemical Co., Ltd.); titanium isopropoxide (Shanghai Maclin Biochemical Technology Co., Ltd.); carbon nanotubes (Jiangsu Tiannai Co., Ltd.); 6 mm thick graphite sheets and 1 mm thick organic glass sheets (Spring New Energy Co., Ltd.); and anion exchange membrane (LE-HoAM Grion 1204 type) and cation exchange membrane (LE-HoAM Grion 0014 type) were purchased from Hangzhou Lvhe Environmental Protection Technology Co., Ltd. All reagents were of analytical grade and did not require further purification.

4.2. Synthesis of FAC-T80/TiO_2. Using a sol−gel/hydrothermal two-step synthesis strategy with Tween 80 as a surfactant, a carbon−titanium composite material was successfully prepared and named FAC-T80/TiO_2. Samples prepared using only the sol−gel method were referred to as AC-T80/TiO_2. As depicted in Figure 8, 2 g of activated carbon was mixed with a 1% Tween 80 ethanol solution (AC-T80) in 100 mL and subjected to 5 min of ultrasonication. Subsequently, 3 mL of titanium isopropoxide was dissolved in an ethanol solution containing 4 M HCl, and the solution was slowly added to the AC-T80 mixture. The mixture was then stirred for 6 h at 50 °C, resulting in a uniform sol−gel solution. The solution was then transferred to a hydrothermal reactor and subjected to hydrothermal treatment at 140 °C for 4 h, followed by natural cooling to room temperature. The resulting product was centrifuged at 8900 rpm three times to separate it from the residual solution. After drying at 60 °C for 12 h, the final powder was ground and stored in a desiccator.

4.3. Material Characterization. The morphology and microstructure of the composite materials were analyzed using a scanning electron microscope (SEM, Regulus 8100). Dynamic changes in wetting behavior were evaluated using a contact angle goniometer (CA-100C). The specific surface area, pore size, and other microsurface characteristics were determined using the ASAP 2020 Analyzer produced by Quantachrome Inc.

4.4. Electrosorption Experiments. A mixture of carbon materials, carbon nanotubes, and deionized water was prepared in specified proportions and sonicated for 35 min at 60% power to achieve a dispersed system. The experimental setup is depicted in Figure 8. Using a response surface methodology, experiments were designed with variations in voltage (0.8−1.6 V), feed flow rate (5−15 mL/min), and feed concentration (250−750 mg/L). Each experimental group comprised 17 experiments, exploring the mutual effects of voltage, feed flow rate, and feed concentration on desalination efficiency. The ion removal rate is calculated as follows

$$\text{ion removal rate (\%)} = \frac{C_0 - C_1}{C_0} \times 100\% = \frac{\kappa_0 - \kappa_1}{\kappa_0} \times 100\%$$

https://doi.org/10.1021/acsomega.3c10498
ACS Omega 2024, 9, 18249−18259

C_0: initial concentration of the solution; C_1: solution concentration after 1 h of device operation; k_0: initial conductivity of the solution; k_1: conductivity of the solution after 1 h of device operation.

4.5. Pilot Electrosorption Testing Equipment. A pilot capacitive deionization (CDI) testing equipment was assembled for long-term stable operation experiments, following the experimental procedure illustrated in Figure 8. Sodium chloride (NaCl) solutions with concentrations of 1000, 2000, 3000, and 4000 mg/L were prepared, and electrosorption experiments were conducted at voltages of 1.2, 1.6, and 2.0 V.

AUTHOR INFORMATION

Corresponding Author

Xiaolong Zhao − *College of Engineering, China University of Petroleum-Beijing AT Karamay, Karamay 834000, China;* orcid.org/0009-0008-6172-2396; Phone: 15265634907; Email: 2432682979@qq.com

Author

Xiangzhi Liu − *College of Chemical Engineering, Shandong Institute of Petroleum and Chemical Technology, Dongying 257000, China*

Complete contact information is available at: https://pubs.acs.org/10.1021/acsomega.3c10498

Notes

The authors declare no competing financial interest.

ACKNOWLEDGMENTS

This work was supported by the Shandong Institute of Petrochemical Technology's Research Start-up Funding Project (2023SS009).

REFERENCES

(1) Vafakhah, S.; Beiramzadeh, Z.; Saeedikhani, M.; Yang, H. Y. A review on free-standing electrodes for energy-effective desalination: Recent advances and perspectives in capacitive deionization. *Desalination* **2020**, *493*, No. 114662.

(2) Oladunni, J.; Zain, J. H.; Hai, A.; Banat, F.; Bharath, G.; Alhseinat, E. A comprehensive review on recently developed carbon based nanocomposites for capacitive deionization: From theory to practice. *Sep. Purif. Technol.* **2018**, *207*, 291−320.

(3) Yang, S. C.; Kim, H. K.; Jeon, S. I.; Choi, J.; Yeo, J. G.; Park, H. R.; Jin, J.; Kim, D. K. Analysis of the desalting performance of flow-electrode capacitive deionization under short-circuited closed cycle operation. *Desalination* **2017**, *424*, 101−121.

(4) Chen, J.; Zuo, K. C.; Li, B.; Hu, J. H.; Liu, W. B.; Xia, D. S.; Lin, L.; Liang, J. J.; Li, X. Y. Fungal hypha-derived freestanding porous carbon pad as a high-capacity electrode for water desalination in membrane capacitive deionization. *Chem. Eng. J.* **2022**, *433* (3), No. 33781.

(5) Lu, T.; Liu, Y.; Xu, X. T.; Pan, L. K.; Alothman, A. A.; Shapter, J.; Wang, Y.; Yamauchi, Y. Highly efficient water desalination by capacitive deionization on biomass-derived porous carbon nanoflakes. *Sep. Purif. Technol.* **2021**, *256*, No. 17771.

(6) Feng, W. M.; Ye, Y. L.; Lei, Z. C.; Feng, C. H.; Wei, C. H.; Chen, S. W. Phenol-degrading sludge as a promising precursor for a capacitive carbon material: Disclosing key factors for the nanostructure and high capacitance. *Carbon* **2018**, *134*, 3−61.

(7) Xu, X. T.; Tan, H. B.; Wang, Z. M.; Wang, C.; Pan, L. K.; Kaneti, Y. V.; Yang, T.; Yamauchi, Y. Extraordinary capacitive deionization performance of highly-ordered mesoporous carbon nano-polyhedra for brackish water desalination. *Environ. Sci.-Nano* **2019**, *6* (3), 981−989.

(8) Yuan, S.-J.; Dai, X. Sewage sludge-based functional nanomaterials: Development and applications. *Environ. Sci.-Nano* **2017**, *4*, 17−26.

(9) Lungile, H.; Zamani, C.; Bhekumuzi, G. Properties of porous carbon electrode material derived from biomass of coffee waste grounds for capacitive deionization. *Mater. Today: Proc.* **2022**, *56* (4), 2178−2183.

(10) Li, C. G.; Li, Y. T.; Yao, Z. H.; Wang, J.; Zhong, Q. A mild approach to bimetallic IF-derived porous carbons as highly efficient oxygen reduction electrocatalysts. *Int. J. Hydrogen Energy* **2021**, *46* (9), 6188−6196.

(11) Xu, X. T.; Liu, Y.; Wang, M.; Yang, X. X.; Zhu, C.; Lu, T.; Zhao, R.; Pan, L. K. Design and fabrication of mesoporous graphene via carbothermal reaction for highly-efficient capacitive deionization. *Electrochim. Acta* **2016**, *188*, 406−413.

(12) Samuel, N.; Wei, T. Electrochemical capacitive behaviors of carbon/titania composite prepared by Tween 80-assisted sol-gel process for capacitive deionization. *Desalination* **2021**, *512*, No. 115131.

(13) Yoon, H. S.; Lee, J. H.; Kim, S. N.; Yoon, J. Y. Review of concepts and applications of electrochemical ion separation (EIONS) process. *Sep. Purif. Technol.* **2019**, *221*, 433−434.

(14) Trócoli, R.; Erinmwingbovo, C.; Mantia, F. L. Optimized lithium recovery from brines by using an electrochemical ion-pumping process based on λ-MnO_2 and nickel hexacyanoferrate. *ChemElectroChem* **2017**, *4*, 143−149.

(15) Zhao, X. Y.; Yang, H. C.; Wang, Y. F.; Sha, Z. L. Review on the electrochemical extraction of lithium from seawater/brine. *J. Electroanal. Chem.* **2019**, *850*, No. 113389.

(16) Zhang, W. J. Structure and performance of $LiFePO_4$ cathode materials: A review. *J. Power Sources* **2011**, *196*, 2962−2970.

(17) Lee, D.-H.; Ryu, T.; Shin, J.; Ryu, J. C.; Chung, K. S.; Kim, Y. H. Selective lithium recovery from aqueous solution using a modified membrane capacitive deionization system. *Hydrometallurgy* **2017**, *173*, 283−288.

(18) Zhao, M. Y.; Ji, Z. Y.; Zhang, Y. G.; Guo, Z. Y.; Zhao, Y. Y.; Liu, J.; Yuan, J. S. Study on lithium extraction from brines based on $LiMn_2O_4$/$Li_{1-x}Mn_2O_4$ by electrochemical method. *Electrochim. Acta* **2017**, *252*, 350−361.

(19) Tang, D. C.; Sun, Y.; Yang, Z. Z.; Ben, L. B.; Gu, L.; Huang, X. J. Surface structure evolution of $LiMn_2O_4$ cathode material upon charge/discharge. *Chem. Mater.* **2014**, *26*, 3535−3543.

(20) Ragavendran, K.; Xia, H.; Mandal, P.; Arof, A. K. Jahn-Teller effect in $LiMn_2O_4$: influence on charge ordering, magnetoresistance and battery performance. *Phys. Chem. Chem. Phys.* **2017**, *19*, 2073−2077.

(21) Kim, J. S.; Kim, K.; Cho, W.; Shin, W. H.; Kanno, R.; Choi, J. W. A truncated manganese spinel cathode for excellent power and lifetime in lithium-ion batteries. *Nano Lett.* **2012**, *12*, 6358−6365.

(22) Wang, L.; Zhang, N.; Wang, Q. TiO_2-modified electrode materials for enhanced electrochemical performance in batteries, fuel cells, and sensors. *J. Mater. Chem. A* **2021**, *9*, 9252−9267.

(23) Liu, Y.; Zhang, J.; Li, Y. Enhancement of electrode wettability and ion transfer by TiO_2 nanoparticle modification for electrochemical applications. *J. Mater. Chem. A* **2019**, *7*, 11020−11030.

(24) Smith, A. B.; Chen, C.; Wang, D. TiO_2-modified electrodes for enhanced ion transfer and electrochemical performance in lithium-ion batteries. *J. Power Sources* **2020**, *452*, No. 227845.

(25) Jones, L. M.; Zhang, X.; Li, N. TiO_2 nanoparticles for improved ion kinetics and electrochemical performance in fuel cells. *ACS Appl. Energy Mater.* **2022**, *5*, 2752−2761.

(26) Wang, Y.; Zhang, L.; Li, J. Enhanced electrochemical performance of TiO_2 nanoparticles by heat treatment for lithium-ion batteries. *J. Alloys Compd.* **2018**, *742*, 854−862.

(27) Chen, D.; Li, Y.; Wang, Q. Impact of heat treatment on the structure and electrochemical performance of TiO_2 nanoparticles for supercapacitor applications. *Ceram. Int.* **2021**, *47*, 19908−19916.

(28) Wu, M. Y.; Li, X. P.; Ge, L. J. Thermal treatment effects on the electrochemical properties of TiO_2 electrodes with enhanced oxygen content. *Ceram. Int.* **2019**, *45*, 6228−6235.

(29) Lu, G. Q.; Wang, G. W.; Wang, P. H.; Yang, Z. Y.; Yan, H.; Ni, W.; Zhang, L.; Yan, Y. M. Enhanced capacitive deionization

performance with carbon electrodes prepared with a modified evaporation casting method. *Desalination* **2016**, *386*, 32−38.
(30) Li, Y.; Li, Z.; Shen, P. K. Simultaneous formation of ultrahigh surface area and three-dimensional hierarchical porous graphene-like networks for fast and highly stable supercapacitors. *Adv. Mater.* **2014**, *26*, 2673−2679.
(31) Saleh, T. A.; Mustaqeem, M.; Khaled, M. Water treatment technologies in removing heavy metal ions from wastewater: A review. *Environ. Nanotechnol., Monit. Manage.* **2022**, *17*, No. 100617.
(32) Tsekov, R.; Pinna, M. Fundamentals of Ion Exchange. In *Ion Exchange and Solvent Extraction: A Series of Advances*; Elsevier, 2019.
(33) Li, H.; Wang, Z.; Chen, L. Enhanced capacitive deionization performance of TiO_2-modified activated carbon electrode. *J. Colloid Interface Sci.* **2019**, *536*, 608−616.
(34) Wang, M.; Xu, X. T.; Li, Y. J.; Lu, T.; Pan, L. K. Enhanced desalination performance of anion-exchange membrane capacitive deionization via effectively utilizing cathode oxidation. *Desalination* **2018**, *443*, 221−227.

https://doi.org/10.1021/acsomega.3c10498
ACS Omega 2024, 9, 18249−18259